

Konrad Mielke^{1,*}
Guixuan Wu^{1,2,*}
Mark Eberhard³
Thomas Kolb⁴
Michael Müller¹


Optimization of Slag Mobility of Biomass Fuels in a Pilot-scale Entrained-Flow Gasifier

The bioliq[®] process, developed at the Karlsruhe Institute for Technology, aims at the production of synthetic fuels and chemicals from biomass. The bioliq[®] technology is based on a two-step process with decentral pyrolysis for the production of a transportable slurry from residual biomass and the central entrained-flow gasification of the slurry by using biomass-to-liquid technology. This study is focused on the slag, which is formed by melting the inorganic ash components during gasification. To operate the gasifier smoothly, a range of desired viscosity has to be defined. A structure-based viscosity model was used to predict the viscosity of the slags at the gasifier outlet. A good agreement between experimental and calculated viscosities is achieved for fully liquid slag systems.

Keywords: Biomass fuels, Entrained-flow gasification, Oxide melts, Slag mobility, Viscosity

Received: November 02, 2020; *revised:* February 26, 2021; *accepted:* May 04, 2021

DOI: 10.1002/ceat.202000531

 This is an open access article under the terms of the Creative Commons Attribution-NonCommercial License, which permits use, distribution and reproduction in any medium, provided the original work is properly cited and is not used for commercial purposes.



Supporting Information
available online

1 Introduction

The synthesis of biofuels by Biomass-to-Liquid (BtL) technologies displays a CO₂-neutral alternative to liquid hydrocarbon fuels, which are derived from fossil energy carriers. The bioliq[®] concept as an example for BtL technologies provides the opportunity to achieve the conversion of low-grade biogenic feedstocks to high-grade synthetic fuels. Usable are dry biogenic feedstocks like straw from agriculture or wood residues. Due to low volumetric energy densities, the feedstocks are pre-treated by fast pyrolysis at temperatures around 500 °C under inert-atmospheric conditions. The end products are char, organic condensates, and noncondensable components. The condensates and the solid char are mixed to form an intermediate fuel called bioSyn crude[®] [1–3].

The bioSyn crude[®] is used as feedstock for the pressurized entrained-flow gasifier in the next step of the process chain to gain a tar-free and low-methane syngas [4–7]. At high temperatures of > 1200 °C and pressures of 40–80 bar, the ash of the slurry melts and forms a slag layer, which flows down the inner reactor wall. On the one hand, this slag protects the refractory material from corrosion (Fig. 1). On the other hand, a slag with high viscosity will block the gasifier outlet. Therefore, the mobility of the slag has to be controlled to prevent stalling of the protective layer at too low viscosity and avoid blockages of the gasifier at too high viscosity [6]. For higher cold gas efficiency and minimizing the heat loss, low operation temperatures are preferred. Hereby, viscosity is one limiting factor because a decrease in operation temperature leads to higher viscosities that could result in the blockage of the outlet and even an unscheduled shutdown of the gasifier.

The slag viscosity is dependent on temperature, pressure, and chemical composition [8–10]. Additionally, the liquidus

temperature has to be considered as a threshold for the start of crystallization, although supercooled melts may remain. Due to crystallization, a partial melt is present consisting of a liquid part and solid crystals. An increasing amount of crystals will influence the viscosity chemically and mechanically [11,12]. Although some viscosity models assume a crystallized part of up to 40 % without significant impact [11], the viscosity behavior induced by crystallization is complex and this needs to be avoided in general during gasification. The impact of slags on the gasification process is depending on the chemical composition of the melt, the form of the crystals, and the environment of melt formation [13,14].

The main chemical component in the investigated slags is the network former SiO₂. According to the common network theory, slags with high SiO₂ contents tend to form supercooled melts characterized by the suppression of crystallization below the liquidus temperature. Therefore, SiO₂-based melts are preferred to guarantee the flow of the slag out of the gasifier.

¹Konrad Mielke, Dr. Guixuan Wu, Dr. Michael Müller
konradmielke@gmail.com

Institute of Energy and Climate Research (IEK-2), Forschungszentrum Jülich GmbH, Wilhelm-Johnen Strasse, 52425 Jülich, Germany.

²Dr. Guixuan Wu
gw@gtt-technologies.de
GTT-Technologies, Kaiserstrasse 103, 52134 Herzogenrath, Germany.

³Mark Eberhard
Karlsruher Institut für Technologie, Institut für Technische Chemie (ITC), P.O. Box 3640, 76021 Karlsruhe, Germany.

⁴Prof. Dr. Thomas Kolb
Karlsruhe Institut für Technologie, Engler-Bunte-Institute, Engler-Bunte-Ring 9a, 76131 Karlsruhe, Germany.

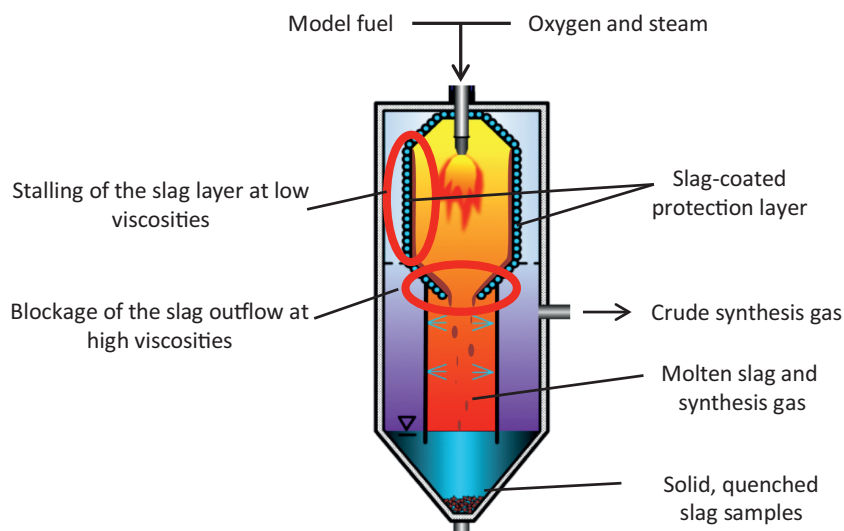


Figure 1. Schematic diagram of an entrained-flow gasifier and slagging.

Unfortunately, these supercooled melts are usually characterized by high viscosity [15]. To achieve the desired low viscosity in the bioliq[®] gasifier, the addition of flux material to the SiO₂-rich feedstock is an established technique. As fluxes alkaline metal oxides, e.g., Na₂O, can be applied, which reduce the viscosity as network modifiers according to the network theory [16].

For the smooth gasifier operation, a viscosity range of 5–25 Pa s inside the gasifier is suggested [17] and has to be achieved by adjusting the chemical composition with fluxing or the temperature. It should be mentioned that the suggested viscosity range is not constant and depends on the individual design of the gasifier. The real-time viscosity values inside the gasifier are difficult to determine because of lacking correspondence for the chemical compositions of feedstock ash, the slag at the reactor wall, and the slag from the outlet of the reactor. Therefore, a range of viscosity instead of a specific value is in general defined as a benchmark for ideal working conditions of the gasifier, in addition to the consideration of the slag as a protective layer of the refractory material from corrosion. Since direct viscosity measurements of the slag at the reactor wall are not feasible, viscosity modeling is proposed as a promising approach to achieve reliable results.

The existing viscosity models for oxide melts can be divided into structure-based and nonstructure-based models. Nonstructure-based models do not consider various structures resulting from interactions between the different components in the slag [18–20]. Therefore, their application is limited for specific systems and temperature ranges. Structure-based models are more complex and take interactions between the slag components into account [21]. Their application is still limited to certain systems [22–24]. To describe the complex influence of slag components on the viscosity of biomass slags, the structure-based model developed by Wu et al. [24–28] was applied in this study.

2 Experimental

2.1 Materials

This study is based on slag samples collected at the outflow of the entrained-flow gasifier, which is integrated in the bioliq[®] process at the KIT [1–3]. Model fuels were prepared to guarantee a constant and well-known chemical composition. Ethylene glycol (Gly) or a pyrolysis oil from beech wood from a barbecue coal production unit “Profagus” (Prof) was used as model liquid phase with similar properties to liquid parts of the bioslurry, e.g., low or no ash content. Na-rich glass pearls from glass-blasting (Na-G) were used as solid phase and display the behavior of the alkali-rich ash content in bioslurries. The chemical composition of the model feedstocks is given in Tab. 1.

For decreasing the viscosity of the slag inside the gasifier, several Na compounds, i.e., Na-oxalate (Na-Ox) and NaOH, were added to the feedstock (Tab. 1). The gasifier operates at temperatures >1200 °C and pressures of 40 bar using oxygen and steam as gasification agents. The slag of the model fuel flows down the reactor wall and exits the reactor with the synthesis gas at the bottom. During the quenching process, the molten slag solidifies and forms solid aggregates, which are used as slag samples for viscosity determination in this study (Fig. 1).

For characterization of the slag samples, the chemical composition of the investigated slags is given in Tab. 2. Due to high-temperature conditions, ash components dominate the composition of the slag samples. According to their chemical composition, two groups were defined. SiO₂-dominated samples are represented by V82 and pure Na-G. The two samples of this group do not differ significantly in chemical composition. Small changes of chemical composition between the samples V82 and pure Na-glass can be caused by regular chemical deviation of samples inside the gasifier.

The second group is the one of Na₂O-enriched samples. Here, Na₂O was added in form of Na-Ox in V79 and as NaOH in V86 and V87 to reduce the slag viscosity. The Na₂O-based fluxes were combined with Na-G to guarantee the formation of a molten slag layer. The addition of NaOH in V86 results in higher Na₂O contents than in V79. The reduced amount of NaOH in V87 leads to lower Na₂O contents.

2.2 Methods

2.2.1 High-Temperature Viscosimetry

The experimental determination of the slag viscosity was conducted by high-temperature viscosimetry. Mo was chosen as material for the crucibles and spindles because of its inert behavior to oxide melts. However, Mo oxidizes at high oxygen partial pressures. Therefore, an Ar/4 vol % H₂ atmosphere was employed to guarantee a sufficient reducing environment

Table 1. Chemical composition of the feedstock.

Chemical composition	Model fuel							
	SL111 (V82)	SL108 (V79)	SL122 (V86)		SL124 (V87)			
	Gly + 4.5 wt % Na-G	Prof + 3 wt % Na-G + 4.5 wt % Na-Ox	Profagus	3 % Na-G	5 % NaOH	Profagus	3 % Na-G	3.3 % NaOH
C [wt %]	36.96	49.96	54.5			54.5		
H [wt %]	9.31	5.41	6.48		0.342	6.48		0.082
N [wt %]	0	0.02	0.12			0.12		
O [wt %] (calculated)	49.23	35.52	38.8		2.721	38.8		0.666
Ash 550 °C	4.5	9.09	0.1	3		0.1	3	
Al ₂ O ₃ [wt %]	0.036	0.042	0.004	0.012		0.004	0.012	
CaO [wt %]	0.466	0.557	0.008	0.294		0.008	0.294	
Fe ₂ O ₃ [wt %]	0.014	0.014	0.026	0.006		0.026	0.006	
K ₂ O [wt %]	0.024	0.135	0.025	0.003		0.025	0.003	
MgO [wt %]	0.187	0.271	0.003	0.099		0.003	0.099	
Na ₂ O [wt %]	0.601	3.852	0.002	0.411	1.937	0.002	0.411	2.557
P ₂ O ₅ [wt %]	0.008	0.009	0.001			0.001		
SO ₃ [wt %]	0.041	0.061	0.018			0.018		
SiO ₂ [wt %]	3.123	4.148	0.014	2.175		0.014	2.175	

Table 2. Chemical composition of investigated slags.

Slag composition	Model fuel				
	SiO ₂ -dominated samples		NaO ₂ -enriched samples		
	Na-G	V82 Gly + 4.5 wt % Na-G	V79 Prof + 3 wt % Na-G + 4.5 wt % NO	V86 Prof + 3 wt % Na-G + 5 wt % NaOH	V87 Prof + 3 wt % Na-G + 3.3 wt % NaOH
Al ₂ O ₃ [wt %]	0.4	0.82	0.68	0.53	0.86
CaO [wt %]	9.78	10.46	6.92	5.63	7
Fe ₂ O ₃ [wt %]	0.2	0.3	0.45	0.43	0.38
K ₂ O [wt %]	0.1	0.52	0.2	0.17	0.39
MgO [wt %]	3.39	4.2	1.75	2.14	3.04
Na ₂ O [wt %]	13.67	13.52	36.24	40.03	31.73
SiO ₂ [wt %]	72.46	70.18	53.76	51.07	56.6
Σ	100	100	100	100	100

during the viscosity measurement. The bioliq[®] slags were grinded to a size of < 1 mm and melted in Mo-crucibles under Ar-H₂. When the necessary amount of molten slag was reached in the crucible, the samples were inserted in the vertical tube furnace of the high-temperature viscosimeter. A rotational viscosimeter RC1 (Rheotec, Germany) was used to determine the viscosity in the temperature range 900–1600 °C. The tempera-

ture was measured with a thermocouple directly below the sample at the bottom of the crucible, and a deviation of approximately 25 °C was observed between the thermocouple and the temperature of the sample inside the crucible, which has been already considered and calibrated before the viscosity measurement. Seebold et al. [12, 15] described the in-house developed instrumental setup (Fig. 2) in detail.

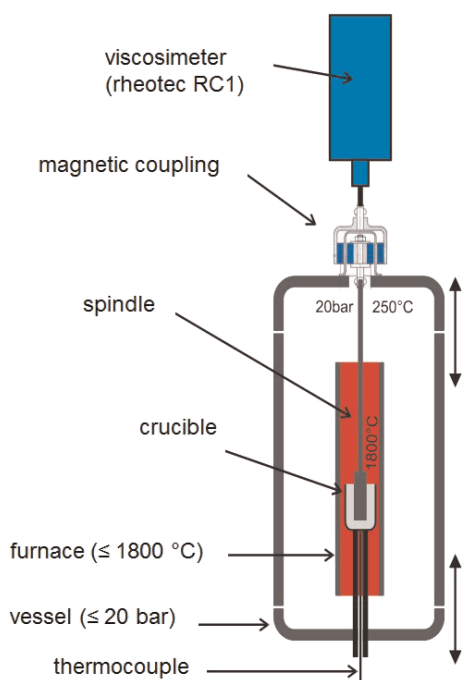


Figure 2. Schematic diagram of the in-house developed viscosimeter.

An automatic measuring program was developed to perform viscosity measurements according to the conditions in Tab. 3. In the temperature range of 900–1600 °C, temperature intervals of 25 °C were defined, and 22 isothermal viscosity measurements were conducted per temperature. During viscosity measurements, the rotational speed was altered from 1 to 400 s⁻¹ and the torque varied accordingly in the range of 0.1–40 mN m. Inaccuracies in the measurement, e.g., due to potential eccentric rotation and even formation of Taylor vortex, were calibrated by a specific device in the calculation of experimental viscosity from the torque measured, which has been described in detail elsewhere [12].

Table 3. Conditions for the experimental determination of the viscosity.

Parameter	Value
Temperature range [°C]	900–1600
Temperature interval [°C]	25
No. of measurements per temperature [-]	22
Rotational speed [s ⁻¹]	1–400
Torque [mN m]	0.1–40

Due to the fact that a decentring rotation of the long spindle could not be completely prevented, the flow behavior in the wide gap was used to calculate the viscosity from torque, rotational speed, and radius of spindle and crucible. Nevertheless, a calibration of the viscosimeter using samples with well-known

viscosities is mandatory. The obtained values show a deviation of approximately 10 % [12].

2.2.2 Viscosity Calculation

The viscosity of the slags investigated was calculated using the structure-based model developed by Wu et al. [25–28], as indicated in Eq. (1). The model not only considers the chemical composition and temperature but also oxygen partial pressure [26, 27]. The used chemical composition is listed in Tab. 2, and a constant oxygen partial pressure of 1 Pa is applied, which approximately corresponds to the atmosphere used in the present study.

Predicting the slag structure is necessary before the viscosity calculation is implemented. Since the viscosity and Gibbs energy have the common structural base [29], the basic structural units in molten slags are described by means of a non-ideal associate solution, which is taken to describe the Gibbs energy of the liquid phase [30]. The distribution of the aforementioned basic structural units at equilibrium was calculated by the software package FactSage using the GTox database [31, 32]. When the formation of potential solid phases was suppressed, the viscosity of supercooled melts was calculated accordingly. As shown in Fig. 3, the resulting viscosity-temperature curves were plotted in combination with the experimental ones. Additionally, the liquidus temperatures (T_L) were marked in Fig. 3, which were calculated by FactSage using GTox database [31, 32] and the SGPS database [33].

$$\ln \eta = \ln \eta_{\text{ideal}} + \ln \eta_{\text{excess}} = \left(\sum_i X_i \ln \eta_i \right) + \left(\ln \eta_{\text{self-pol.}} + \ln \eta_{\text{inter-pol.}} \right) \quad (1)$$

where

$$\ln \eta_i = A_i + B_i/T \quad (2)$$

$$\ln \eta_{\text{self-pol.}} = \sum_j \left(A_{(\text{SiO}_2)_j} + B_{(\text{SiO}_2)_j}/T \right) \left(X_{\text{SiO}_2}^{n_j} \right) + \dots, \quad (3)$$

$j = 1$ and 2

$$\ln \eta_{\text{inter-pol.}} = \sum_m \left(A_{(\text{Si-Al})_m} + B_{(\text{Si-Al})_m}/T \right) \left(X_{(\text{Si-Al})_m} X_{\text{SiO}_2}^{n_m} \right) + \dots,$$

$m = 1, 2, 3 \dots$

(4)

(Si-Al)_m is the silicon-aluminum-based ternary associate species. η_{ideal} and η_{excess} are the ideal viscosity and the excess viscosity, respectively; X_i is the mole fraction of the associate species i ; η_i is the viscosity contribution from the associate species i ; $\eta_{\text{self-pol.}}$ is the excess viscosity due to the critical silicate related self-polymerizations; $\eta_{\text{inter-pol.}}$ is the excess viscosity due to the critical inter-polymerizations; n_j and n_m are the integer coefficients that relate to a particular degree of polymerization;

A_i and B_i are the temperature- and composition-independent constants, respectively, for the ideal viscosity; $A_{(\text{SiO}_2)_m}$ and $A_{(\text{Si-Al})_m}$ are the temperature-independent constants for the excess viscosity; $B_{(\text{SiO}_2)_m}$ and $B_{(\text{Si-Al})_m}$ are the composition-independent constants for the excess viscosity; T is the absolute temperature; $X_{\text{SiO}_2}^m$ and $(X_{(\text{Si-Al})_m} X_{\text{SiO}_2}^m)$ are the composition-dependent weighting factors for the contribution of relatively large clusters derived from the associate species to the excess viscosity. It is worth mentioning that other terms relevant to the excess viscosity are not given here but are described in detail elsewhere [26,27].

3 Results and Discussion

In Fig. 3, the viscosity values calculated by the model (calc.) are compared with experimentally determined viscosities (exp.). It is seen that the viscosity of supercooled melts (sc.) is also given. Attention should be paid to the experimental viscosity data below the liquidus temperature, where the formation of potential crystals influences the flow behavior of the melt.

The SiO_2 -dominated group is characterized by a gradual decrease of the logarithmic viscosity with increasing temperature. In the range of 1300–1450 °C, the desired viscosity of 5–25 Pa s [17] is achieved for the slag sample of Na-rich glass. This implicates that a temperature variation or fluctuation within 150 °C is allowed during the operation of entrained-flow gasifiers for the investigated feedstocks.

The similar chemical composition of samples from the SiO_2 -dominated group (V82, Na-G) results in nearly similar viscosities (Fig. 3). It is noticed that the viscosity of Na-G with higher

SiO_2 content is greater than that of V82. The higher SiO_2 content also causes a higher liquidus point. The calculated and experimental viscosity values agree very well at the temperature range investigated. This indicates that the model performance is good for the SiO_2 -dominated slags and the experimental determination of these slags is not necessary for each sample.

For the calculated values, the addition of 4.5 % Na-oxalate in V79 results in a significant reduction of the viscosity values. This effect is enhanced in V86 by further increasing the amount of Na_2O . The lower Na_2O content in V87 results in higher viscosities than in V79 and V86. The experimental and calculated viscosities are not always in good agreement over the entire temperature range investigated. For example, the experimental viscosity of V87 remains higher up to 975 °C. When exceeding this temperature, the viscosity decreases significantly in the experiment and causes the viscosity even to be lower than the ones of V79 in contrast to the calculated values.

The low viscosities of this Na_2O -enriched group allow lower operation temperatures, i.e., around 1000 °C, to achieve the desired slag viscosity. However, only a small temperature variation of approx. 20 °C is allowed to achieve the desired viscosity of 5–25 Pa s because of a sharp increase of viscosity by decreasing temperature. Moreover, the viscosities were determined in supercooled melts and a noticeable crystallization was observed at temperatures around 1000 °C significantly below the liquidus temperature T_L .

The increasing crystallized phases at lower temperatures may cause the change from Newtonian to Non-Newtonian flow behavior below the value of critical viscosity. The averaged viscosity value below the critical viscosity is much more inaccurate and causes a deviation of the experimental data from the calculated viscosity values. It is worth noting that the experimental values were collected only to 900 °C, because at lower temperatures the maximum torque allowed by the viscosimeter was reached. Additionally, the corrosion of the thermoelements can intensify in this temperature range.

3.1 Influence of Na_2O on Melting Behavior and Viscosity

The addition of Na_2O causes a strong increase of viscosity with decreasing temperature. This effect is reflected in the experimental results but not in the calculated ones. The calculated phase equilibrium for V79 explains this deviation (Fig. 4). Calculated phase equilibria for the other investigated slags can be found in the Supplementary Information (S1–S3). The FactSage calculation shows stable crystals, e.g., silicates $\text{Na}_4\text{CaSi}_3\text{O}_9$, in the melt at temperatures below 1125 °C in V79, V86, and V87. These crystals cause an increase

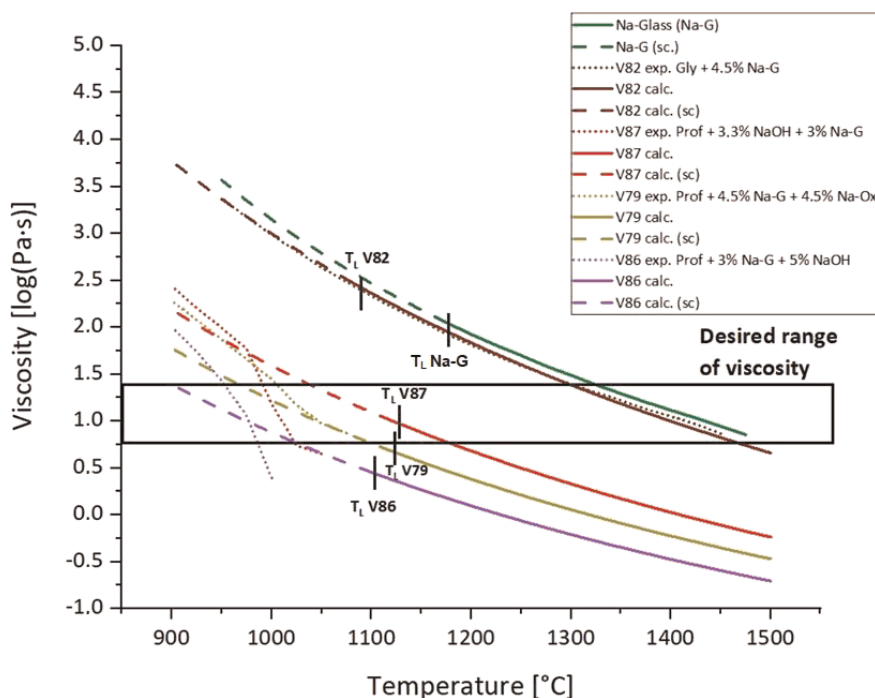


Figure 3. Experimental (exp.) and calculated (calc.) viscosities of chosen bioliq® slags with definition of the supercooled melts (sc.).

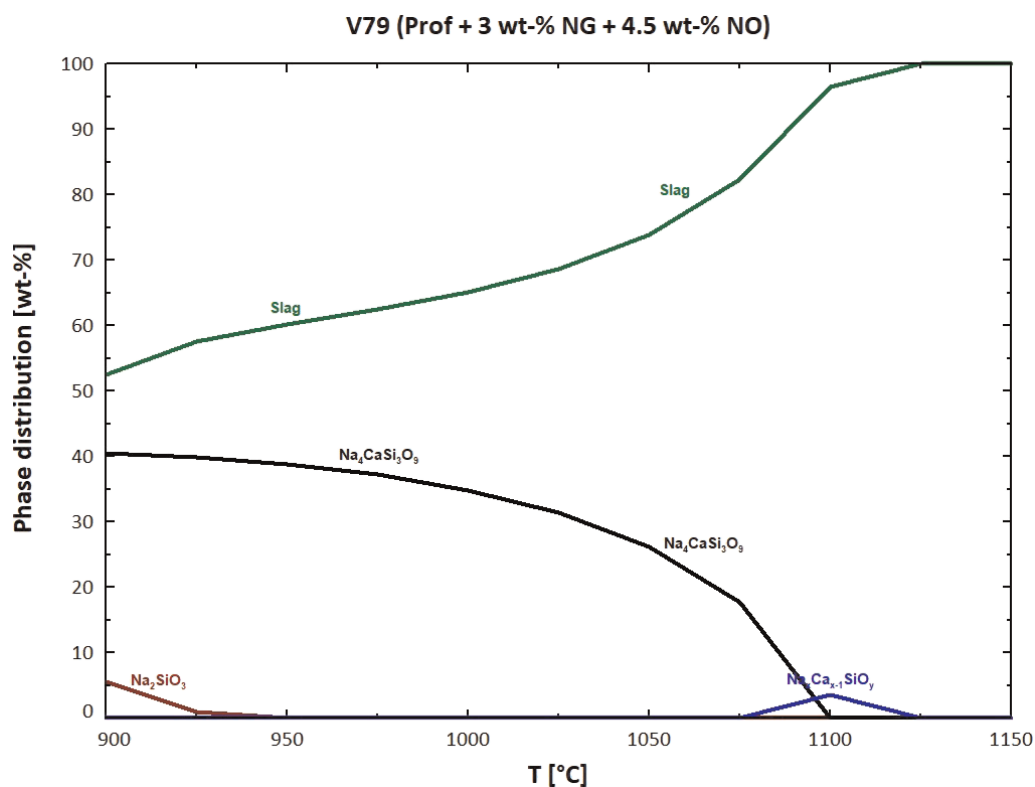


Figure 4. Phase distribution of the slag V79 with respect to temperature at equilibrium.

of viscosity because of mechanical resistance of the formed crystals dependent on the shape [11, 34, 35] which results in an inconsistent flow behavior [36, 37]. Furthermore, the crystallization leads to a significant decrease in Na_2O content in the melt. Thus, the viscosity of the remaining melt is also increased due to less Na_2O as a network modifier available to reduce the viscosity. That means, the reasons for the viscosity increase due to crystallization are two-fold, i.e., from physical and chemical effects as reported by Seebold et al. [12].

The calculated viscosities for V79 are in good agreement with the experimental values at temperatures above 1050°C (Fig. 3). The agreement between experimental and calculated viscosities at temperatures of $1025\text{--}1075^\circ\text{C}$ indicates the presence of supercooled melts, which occurs up to 100°C below the liquidus temperature T_L . In other words, a supercooling degree of approx. 75°C is required to induce the occurrence of crystallization. Since the viscosity model assumes a supercooled melt without crystallization, the calculated values are lower than the experimental values at low temperatures, when crystallization occurs. Additionally, it is noticed that at high temperatures the experimental viscosities of V86 and V87 are respectively lower than the calculated ones of these samples, possibly due to the higher Na_2O content in melts than expected.

3.2 Relation Between the Determined Slag Viscosities and the Flow Behavior of the Slags in the Gasifier

The operating temperature of the gasifier is estimated by an equilibrium temperature calculated with the flow sheet simulation software ASPEN. The temperature of the moving slag at the reactor wall is derived from the operating temperature and supported by the results of CFD modeling [38–40]. The calculated slag temperatures in Tab. 3 are compared with that corresponding to the desired range of viscosity indicated in Fig. 3. For the SiO_2 -dominated sample V82 the temperature of the moving slag is estimated at 1350°C during the gasification. This corresponds well with the temperature range of $1300\text{--}1450^\circ\text{C}$, which is preferred concerning the viscosity conditions and results in the reduction of slag-related problems during the gasification of these samples.

The applied temperatures during gasification for the Na_2O -enriched slags (V79, V86, and V87) are in the range of $1250\text{--}1350^\circ\text{C}$ and exceed the temperatures for the desired viscosity range of these samples ($950\text{--}1050^\circ\text{C}$) significantly (Tab. 4). As displayed in Fig. 3, the viscosities are significantly lower than the desired values at the applied temperature conditions. Such low viscosities may cause the stalling of the protective slag layer (Fig. 1). The viscosity can be increased as the temperature declines. However, the relatively high temperatures are necessary to avoid the blockage of the gasifier outlet by crystallization. As an alternative, the adjustment of slag composition is therefore considered, e.g., by adding more silica or less Na.

Table 4. Temperatures of the slags in the bioliq[®] gasifier.

	V79	V82	V86	V87
Estimated temperature of the moving slag at the gasifier wall during gasification [°C]	1363	1350	1277	1294
Desired temperature range concerning slag viscosity [°C]	1010–1075	1300–1450	950–980	1020–1040

It should be mentioned that there is a possible difference between the chemical composition of the quenched slag in the gasifier outflow and that at the reactor wall inside the gasifier. This may result in a deviation of slag mobility inside the gasifier from that determined experimentally using the quenched slags or the corresponding model prediction. The specific influence of the position at the reactor wall to the content of the main slag-forming components Na₂O, SiO₂, K₂O, and CaO is demonstrated for sample V81 (Fig. 5), taken as an example with similar composition to sample V82.

Fig. 5 illustrates that there is a slight increase in the SiO₂ content at the position MP5, which is associated with a decrease of CaO, Na₂O, and K₂O content at the same position. These changes in chemical composition in the vertical direction are regular fluctuations and can appear at any position of the gasifier. The influence of different radial positions (MP1–4) on the slag composition was also investigated and the results indicate a limited influence to the slag composition.

Based on the chemical composition obtained, the viscosities were calculated with the model (Fig. 6). The difference in the chemical composition results in different magnitudes of the viscosity data at the same temperature. The slag at MP5 has the highest viscosity because of the highest SiO₂ content. The viscosity at the other measuring points are close to each other according to the small differences in their chemical composition.

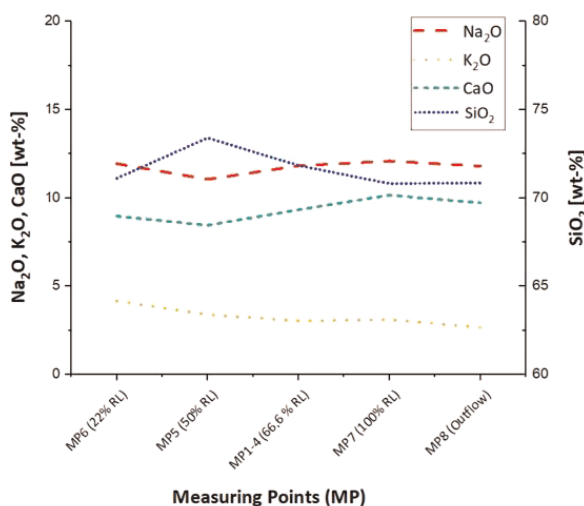


Figure 5. Change of chemical composition depending on sampling position of V81.

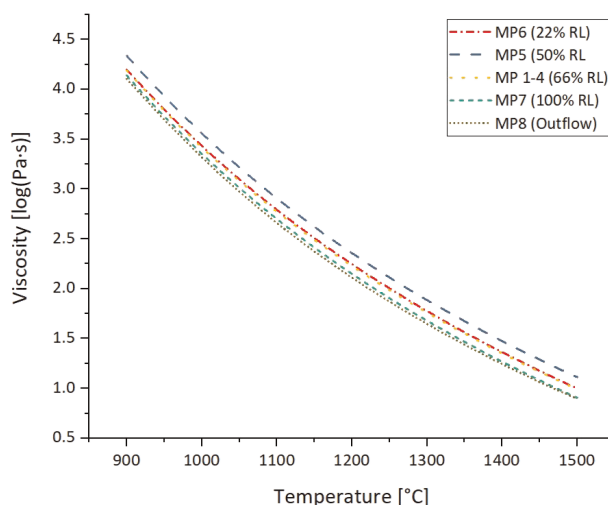
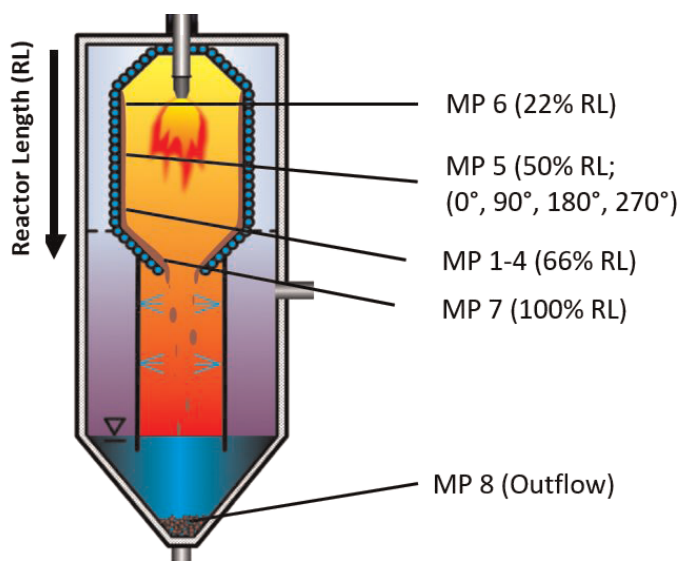


Figure 6. Change of viscosity depending on sampling position of V81.

3.3 Application of Viscosity Prediction in the Adjustment of Slag Composition

This study aims to achieve the desired range of viscosity inside the gasifier via the adjustment of temperature or composition. The viscosity modeling enables this adjustment in advance, which can then be validated with a limited amount of experimental work. Fig. 7, as an example, is plotted with MATLAB[®], where the iso-viscosity data matrix is generated using a self-built solver by setting two variables including chemical composition and temperature of slags. This enables the determination of the necessary temperature to reach the given viscosity for the investigated samples. In the example the maximum viscosity value of 25 Pa s in entrained-flow gasifiers [17] was chosen to define a threshold for the minimal temperature to operate the gasifier economically without viscosity-related problems.



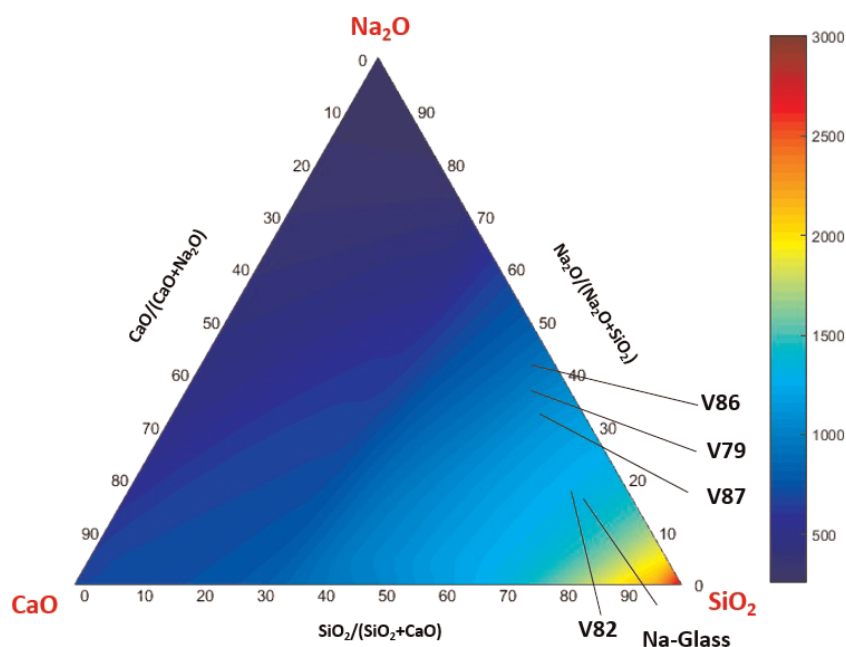


Figure 7. Ternary diagram for relation between chemical composition (mol %) in the system SiO_2 - CaO - Na_2O and temperature ($^\circ\text{C}$) at a constant viscosity value of 25 Pa s, where the influence of potential crystallization is not considered.

The three main components (SiO_2 , Na_2O , and CaO) in the investigated slags (V79, V82, V86, and V87) are chosen to be composition variables, and other minor components are not considered in the ternary diagram.

According to Fig. 7, it is easy to determine the required temperature for different slag candidates in order to achieve the desired viscosity. In the other way around, the chemical composition of the feedstock can also be adjusted for a fixed temperature and viscosity. This enables to design a target-oriented fluxing for the preferred viscosity range under the condition that the ash content of the feedstock and slag does not differ significantly.

For the SiO_2 -dominated group (Na-rich glass and V82) higher temperatures are required to achieve the desired viscosity (Fig. 7). This agrees well with both the calculated and experimental results in this investigation due to the relatively high content of the network former SiO_2 . In contrast, the samples of the Na_2O -enriched group (V79, V86, and V87) can achieve the desired viscosity at lower temperatures due to the higher content of the network modifier Na_2O . The addition of CaO also modifies the slag network structure and leads to a slight decrease in viscosity. However, the formation of potential Ca-based phases with high melting point will cause a higher risk of crystallization, which is not considered in this figure.

The impact of the two main parameters, i.e., slag composition and temperature, on the viscosity during the entrained-flow gasification is clearly visualized in Fig. 7. To optimize the efficiency of entrained-flow gasifiers, such visualization can be employed to adjust the slag composition in order to reach low viscosities at low temperatures. It should be pointed out that more than three components can be taken into account in the visualization in order to provide more accurate data for real slags.

4 Conclusion

The mobility of slags is an important parameter for operating an entrained-flow gasifier. With consideration of minimizing the corrosion on the wall material, achieving the optimal viscosity range guarantees the efficient operation of the reactor without blocking the outflow. To adjust this viscosity range, the structure-based viscosity model is adopted, using the chemical composition of slag collected at the outflow of the gasifier. For the evaluation of the model the viscosity of these slags was also determined experimentally.

The composition of slag from the outflow does not differ significantly from that at the wall inside the reactor. Nevertheless, even small deviations in chemical composition sometimes can result in significant different viscosities.

The investigated slags are characterized by high SiO_2 or Na_2O contents. SiO_2 -dominated slags are characterized by high viscosities, which can be significantly decreased by the addition of Na_2O . The improvement of the economic efficiency is achieved by

lowering the operation temperature, where the adjustment of slag composition is challenging in order to obtain the optimal viscosity range. Attention should be paid to the risk in a sharp viscosity increase caused by crystallization at lower temperatures. Therefore, the gasification temperature for Na_2O -enriched systems is suggested to be higher than supposed by viscosity calculations.

The results of this investigation can be applied to adjust the temperature or chemical composition in order to achieve a desired viscosity range. The viscosity-temperature-composition relations are visualized in the ternary diagram, where three major slag components, namely, SiO_2 , CaO , and Na_2O , in this study are chosen and taken as an example. Such visualization enables to simplify the adjustment, although the results obtained are only the basis for further investigations. This provides a guideline to optimize the flow behavior of several biomass slags in entrained-flow gasification.

Supporting Information

Supporting Information for this article can be found under DOI: <https://doi.org/10.1002/ceat.202000531>.

Acknowledgment

The authors gratefully acknowledge the financial support by the Helmholtz Association of German Research Centres (HGF) in the frame of the Helmholtz Virtual Institute for Gasification Technology HVIGasTech (VH-VI-429), the Fachagentur für Nachwachsende Rohstoffe (FNR) for funding the bioliq[®] pilot

plant, the Wirtschaftsministerium of Baden Württemberg for financial support, and our industry cooperation partner and plant manufacturer Air Liquide for financial support and consulting. Open access funding enabled and organized by Projekt DEAL.

The authors have declared no conflict of interest.

Abbreviations

BtL	biomass-to-liquid
Gly	ethylene glycol
Na-G	sodium-rich glass
Na-Ox	Na-oxalate

References

- [1] N. Dahmen, J. Abeln, M. Eberhard, T. Kolb, H. Leibold, J. Sauer, D. Stapf, B. Zimmerlin, *WIREs Energy Environ.* **2016**, *6* (3), 1–10.
- [2] T. Kolb, M. Eberhard, N. Dahmen, H. Leibold, M. Neuberger, J. Sauer, H. Seifert, B. Zimmerlin, *DGMK-Tagungsbericht* **2013**, *2*, 81–87.
- [3] T. Nicoleit, N. Dahmen, J. Sauer, *Energy Technol.* **2016**, *4* (1), 211–229.
- [4] M. Eberhard, U. Santo, D. Böning, H. Schmid, B. Michelfelder, B. Zimmerlin, A. Günther, P. Weigand, M. Müller-Hagedorn, D. Stapf, T. Kolb, *Chem. Ing. Tech.* **2018**, *90* (1–2), 85–98.
- [5] Q. Fradet, M. Braun-Unkhoff, U. Riedel, *Energy Fuels* **2018**, *32* (12), 12532–12544.
- [6] T. Kolb, M. Aigner, R. Kneer, M. Müller, R. Weber, N. Djordjevic, *J. Energy Inst.* **2016**, *89* (4), 485–503.
- [7] A. Mueller, P. Stoesser, T. Kolb, in *39th Int. Technical Conf. on Clean Coal and Fuel Systems 2014*, Coal Technologies Associates, Gaithersburg, MD **2014**, 744–755.
- [8] S. Arvelakis, F. J. Frandsen, K. Dam-Johansen, in *Proc. of the 30th Int. Technical Conf. on Coal Utilization & Fuel Systems*, Coal Technology Association, Gaithersburg, MD **2005**, 1215–1225.
- [9] J. Gao, G. Wen, T. Huang, P. Tang, Q. Liu, *J. Non-Cryst. Solids* **2016**, *435*, 33–39.
- [10] M. W. Nichols, A. P. Lingras, D. Apelian, in *Proc. of the 2nd Int. Symp. on Metall. Slags and Fluxes*, TMS-AIME, Warrendale, PA **1984**, 235–251.
- [11] A. Kondratiev, E. Jak, P. C. Hayes, *JOM* **2002**, *54* (11), 41–45.
- [12] S. Seebold, G. Wu, M. Müller, *Fuel* **2017**, *187*, 376–387.
- [13] J. W. Nowok, J. P. Hurley, D. C. Stanley, *Energy Fuels* **1993**, *7* (6), 1135–1140.
- [14] R. Roscoe, *J. Phys. Colloid Chem.* **1952**, *52*, 267–269.
- [15] S. Seebold, M. Eberhard, G. Wu, E. Yazhenskikh, D. Sergeev, T. Kolb, M. Müller, *Fuel* **2017**, *197*, 596–604.
- [16] W. J. Zachariasen, *J. Am. Ceram. Soc.* **1932**, *54*, 3841.
- [17] *Gasification* (Eds: C. Higman, M. van der Burgt), Elsevier, Burlington, MA **2003**.
- [18] A. Kondratiev, E. Jak, *Metall. Mater. Trans. B* **2001**, *32* (6), 1015–1025.
- [19] H. Shaw, *Am. J. Sci.* **1972**, *272* (9), 870–893.
- [20] G. Urbain, *Trans. Br. Ceram. Soc.* **1981**, *80*, 139–141.
- [21] K. Hack, G. Wu, E. Yazhenskikh, T. Jantzen, M. Müller, *Calphad: Comput. Coupling Phase Diagrams Thermochem.* **2019**, *65*, 101–110.
- [22] I. Avramov, C. Rüssel, R. Keding, *J. Non-Cryst. Solids* **2003**, *324* (1), 29–35.
- [23] A. Kondratiev, P. C. Hayes, E. Jak, *ISIJ Int.* **2006**, *46* (3), 359–367.
- [24] D. Sichen, J. Bygd'en, S. Seetharaman, *Metall. Mater. Trans. B* **1994**, *25* (4), 519–525.
- [25] G. Wu, E. Yazhenskikh, K. Hack, M. Müller, *Fuel Process. Technol.* **2015**, *138*, 520–533.
- [26] G. Wu, S. Seebold, E. Yazhenskikh, K. Hack, M. Müller, *Appl. Energy* **2019**, *236*, 837–849.
- [27] G. Wu, S. Seebold, E. Yazhenskikh, K. Hack, M. Müller, *Fuel Process. Technol.* **2018**, *171*, 339–349.
- [28] G. Wu, E. Yazhenskikh, K. Hack, E. Wosch, M. Müller, *Fuel Process. Technol.* **2015**, *137*, 93–103.
- [29] R. E. Aune, S. Sridhar, M. Hayashi, *High Temp. Mater. Processes* **2003**, *22* (5–6), 369.
- [30] E. Yazhenskikh, K. Hack, M. Müller, *Calphad: Comput. Coupling Phase Diagrams Thermochem.* **2008**, *32* (3), 506–513.
- [31] C. W. Bale, E. Bélisle, P. Chartrand, S. A. Decterov, G. Eriksson, A. E. Gheribi, K. Hack, I.-H. Jung, Y.-B. Kang, J. Melançon, A. D. Pelton, S. Petersen, C. Robelin, J. Sangster, P. Spencer, M.-A. Van Ende, *Calphad: Comput. Coupling Phase Diagrams Thermochem.*, **2016**, *55*, 1–19.
- [32] *Database GTOx*, GTT-Technologies, Herzogenrath, Germany **2010–2019**.
- [33] *SGPS – SGTE Pure Substances Database (v13.1)*, SGTE, Saint Sulpice, France **2017**.
- [34] J. P. Schupsky, M. Guo, B. Blanpain, M. Müller, *J. Sustainable Metall.* **2020**, *6* (2), 216–226.
- [35] J. P. Schupsky, O. Saar, G. Wu, M. Dohrn, M. Müller, *Fuel* **2020**, *280*, 118663.
- [36] A. Einstein, *Ann. Phys.* **1906**, *19*, 289–306.
- [37] A. Einstein, *Ann. Phys.* **1911**, *34*, 591–592.
- [38] S. Fleck, U. Santo, C. Hotz, T. Jakobs, G. Eckel, M. Mancini, R. Weber, T. Kolb, *Fuel* **2018**, *217*, 306–319.
- [39] M. Mancini, M. Alberti, M. Dammann, U. Santo, G. Eckel, T. Kolb, R. Weber, *Fuel* **2018**, *225*, 596–611.
- [40] M. Mancini, R. Weber, P. Weigand, W. Leuckel, T. Kolb, *26. Deutscher Flammentag: Verbrennung und Feuerung*, VDI-Berichte, Vol. 2161, VDI-Verlag, Düsseldorf **2013**, 625–634.

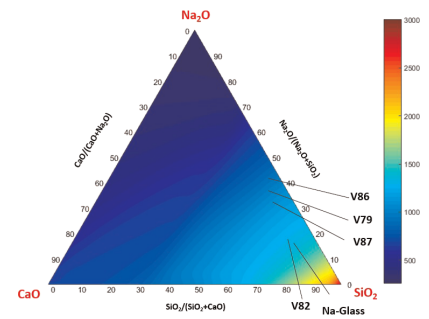
Research Article: The slag, which is formed by melting the ash components of a bioslurry during entrained-flow gasification, is investigated. As a range of desired viscosity of the slag has to be defined for a smooth gasifier operation, the viscosity was determined experimentally and by modeling. The results provide a guideline to optimize the flow behavior of several biomass slags in entrained-flow gasification.

Optimization of Slag Mobility of Biomass Fuels in a Pilot-scale Entrained-Flow Gasifier

Konrad Mielke*, Guixuan Wu*, Mark Eberhard, Thomas Kolb, Michael Müller

Chem. Eng. Technol. **2021**, *44* (7), XXX ... XXX

DOI: 10.1002/ceat.202000531



Supporting Information
available online